Elastic properties of 2D ultrathin tungsten nitride crystals grown by chemical vapor deposition

Wang, Hong; Sandoz-Rosado, Emil J.; Tsang, Siu Hon; Lin, Jinjun; Zhu, Minmin; Mallick, Govind; Liu, Zheng; Teo, Edwin Hang Tong

2019

Wang, H., Sandoz-Rosado, E. J., Tsang, S. H., Lin, J., Zhu, M., Mallick, G., . . . Teo, E. H. T. (2019). Elastic properties of 2D Ultrathin tungsten nitride crystals grown by chemical vapor deposition. Advanced Functional Materials, 29(31), 1902663-. doi:10.1002/adfm.201902663

https://hdl.handle.net/10356/142547

https://doi.org/10.1002/adfm.201902663

Elastic Properties of 2D Ultrathin Tungsten Nitride Crystals Grown by Chemical Vapor Deposition

Hong Wang, Emil J. Sandoz-Rosado, Siu Hon Tsang, Jinjun Lin, Minmin Zhu, Govind Mallick, Zheng Liu*, and Edwin Hang Tong Teo**

Dr. H. Wang, Mr. J. Lin, Dr. M. Zhu, Prof. E. H. T. Teo
School of Electrical and Electronic Engineering
Nanyang Technological University, 50 Nanyang Avenue, 639798, Singapore
E-mail: htteo@ntu.edu.sg

Dr. E. J. Sandoz-Rosado, Dr. G. Mallick
Weapons and Materials Research Directorate, U. S. Army Research Laboratory
Aberdeen Proving Ground (APG), Maryland 21005, USA
E-mail: govinda.mallick.civ@mail.mil

Dr. S. H. Tsang
Temasek Laboratories@NTU, Nanyang Technological University, 637553, Singapore

Prof. Z. Liu
School of Materials Science and Engineering
Nanyang Technological University, 50 Nanyang Avenue, 639798, Singapore
E-mail: z.liu@ntu.edu.sg

Keywords: (2D material, tungsten nitride, chemical vapor deposition, Young's modulus, atomic force microscopy)

3D transition metal nitrides are well recognized for their good electrical conductivity, superior mechanical properties and high chemical stability. Recently, 2D transition metal nitrides have been successfully prepared in the form of nanosheets and show potential application in energy storage. However, the synthesis of highly crystalline and well-shaped 2D nitrides layers is still in demand for the investigation of their intrinsic physical properties. Here we report the growth of ultrathin tungsten nitride crystals on SiO_2/Si substrates by a salt-assisted chemical vapor deposition (CVD) method. High-resolution transmission microscopy verifies the as-grown samples are highly

crystalline WN. The stiffness of ultrathin WN is investigated by atomic force microscopy based nanoindentation with the film suspended on circular holes. The 3D Young's modulus of few-layer (4.5 nm thick or more) WN is determined to be $3.9 \times 10^2 \pm 1.6 \times 10^2$ GPa, which is comparable with the best experimental reported values in 2D family except graphene and h-BN. The synthesis approach presented in this paper offers possibilities of producing and utilizing other highly crystalline 2D transition-metal nitride crystals.

1. Introduction

Following the discovery of graphene, a number of other 2D members including transition metal dichalcogenides (TMDs), black phosphorus (BP) and transition metal carbides with diverse properties have joined the 2D family and attracted great research interests.[1-6] At the same time, the research community shows consistent enthusiasm in exploring new 2D materials with intriguing physical properties and functionalities.[7-13] 2D transition metal nitrides are the latest additions to the 2D family.[14-16] Transition metal nitrides in its bulk form are refractory compounds with good electrical conductivity, high chemical stability and superior mechanical properties (Young's modulus and hardness).[17-18] Among them, tungsten nitride (WN) films are potentially useful as diffusion barriers in electronics and protective coatings.[19-20] However, up to date, most of the 2D transition metal nitrides (MXene-Ti_4N_3,[14] MoN,[15] W_2N,[15] V_2N[15] and Mn_3N_2[16]) are synthesized in the form of nanosheets in solutions, either by etching a MAX phase precursor, or by an ammoniation method. Solution-related process may result in nitrides nanosheets with functional groups on its surface, which makes the investigation of the intrinsic physical properties of these 2D nitride a challenging task. Recently, Wang et al. used a metal immiscibility route to grow 2D TaN crystals on copper surface.[21] Currently, direct deposition of well-shaped 2D WN

crystals on substrates still remains a challenge. On the other side, transition metal nitrides are well-known for their superior mechanical properties. What happens to the Young's moduli of nitrides when their thicknesses reduce to 2D limits is not only interesting for fundamental research but also important for potential applications of 2D nitrides in ultrathin protective coatings.[20]

In this context, we report the growth of atomically-thin WN crystals on SiO_2/Si substrates by salt-assisted CVD — a method recently described for universal synthesis of 2D metal chalcogenides.[22-27] The sample thickness could be tuned by changing the concentration of ammonia during reaction. By suspending the as-grown film on a hole and bending it with the tip of an atomic force microscope (AFM), the average Young's modulus of the 2D few-layer WN is determined to be around 3.9×10^2 GPa, which is only lower than that of graphene and h-BN in the 2D family.[28-30]

2. Results and Discussion

The illustration of the material growth setup is shown in **Figure 1a**. Briefly, precursors consisting of well-mixed WO_3 and NaCl powders are loaded in an alumina crucible into the center of a tube furnace. At the growth temperature, NH_3 is introduced for the ammoniation reaction and the deposition of WN crystals on the substrate positioned slightly above the solid precursors. As deposited WN crystals show nearly triangular or other shapes with uniform color contrast on SiO_2/Si substrates. The typical thickness of the layers is around 3 nm, as suggested by the AFM image shown in Figure 1c. However, a small nucleus with much larger thickness is present in the center of each crystal (Figure 1b). X-ray photoelectron spectroscopy (XPS) is used to examine the chemical states of the as-grown WN layers. The XPS survey spectra for ultrathin WN crystals deposited at a SiO_2/Si substrate is shown in Figure S1. The high-resolution W 4f core levels spectrum is fitted with four peaks corresponding to the following components: nitrided W (32.2

eV, W $4f_{7/2}$; 34.4 eV, W $4f_{5/2}$) and oxidized W (35.4 eV, W $4f_{7/2}$; 37.6 eV, W $4f_{5/2}$), as shown in Figure S2.[31-32] The slightly oxidized W probably forms on the surface of WN layers because of the enhanced air instability when layer thickness is decreased to the 2D limit. Besides, the N 1s core levels spectrum is fitted with two components with the corresponding binding energies centered at about 397.1 eV and 400.0 eV. While the high-intensity 397.1 eV component corresponds to the W-N bond, the small hump peak at 400.0 eV comes from the small quantity N atoms or molecules present in interstitial sites of tungsten nitride.[31-32] Both the W and N XPS spectra agree very well with previous reported results in tungsten nitride films deposited by other methods.[31-33] The XPS analysis thus verifies that the as-grown ultrathin crystals are tungsten nitride.

The crystallographic structure of the as-deposited crystals is characterized by transmission electron microscopy (TEM) and selected-area electron diffraction (SAED). Figure 1d shows the edge of an ultrathin WN crystal transferred to TEM grid. Tungsten nitride crystallizes normally in two distinct forms of cubic W_2N (a_0 = 4.128 Å) and hexagonal WN (a_0 = 2.895 Å, c_0 = 2.826 Å). In the high-resolution TEM (HRTEM) image (Figure 1e), clear lattice fringes are visible with distance of 2.5 Å, consistent with the interlayer separation (2.505 Å) of the (100) crystal plane of hexagonal WN. This conclusion is further confirmed by the lattice distances and their mutual angles measured from the diffraction patterns (Figure 1f), which are in perfect agreement with the hexagonal WN structure. Furthermore, the well-defined lattice fringes and sharp diffraction spots indicate that the film are highly crystallized.

In the CVD synthesis process, no WN nucleation and growth occurs on substrates without the use of salt (Figure S3), which suggests that the salt plays an important role in the growth of 2D WN. Salt-assisted CVD growth has been employed for the deposition of more than 40 2D metal

chalcogenides on substrates and the growth mechanism has been investigated in both theoretical and experimental aspects.[22-24, 34] Rasouli et al. demonstrated that the salt reacts with WO_3 to form intermediate tungsten-oxychloride compounds.[34] Compared with the high-melting-point WO_3, tungsten-oxychloride compounds are volatile and serve as ideal precursor for the vapor-phase deposition of 2D tungsten-chalcogenides. Our work suggests that the salt-assisted method could also be applied for 2D nitrides synthesis. Furthermore, compared with the salt-assisted CVD growth of 2D chalcogenides, the synthesis of 2D nitrides are more controllable because a gaseous precursor − ammonia is used in the reaction, instead of the solid S, Se and/or Te precursors in the metal chalcogenides synthesis. In fact, the thickness of 2D WN crystals can be easily controlled by adjusting the concentration of NH_3 in the carrier gas. Figure 2a-c display the typical optical images of WN crystals deposited with varied NH_3 concentrations (12 - 40% by volume), while keeping other synthesis parameters identical. WN layers as thin as 3 nm can be deposited with a low NH_3 concentration of 12% (Figure 2a). Increasing the concentration to 15% allows the formation of few-layer WN with thickness between 4 to 6.5 nm (Figure 2b). The AFM images (height profiles) of WN crystals with 5 nm and 6.3 nm thicknesses are shown in Figure 2e (Figure S4a) and 2f (Figure S4b), respectively.

In addition to the atomically flat 2D WN, a small dot identified as the nucleation site is observed in the center of each WN crystal, even for the thinnest sample in Figure 2a. These nuclei centers also get larger and thicker with increasing NH_3 concentration, and become brown or black in color under optical microscope (Figure 2b and 2c). High-magnification SEM image (lower inset of Figure 2c) suggests that the brown or black nuclei are vertically grown three-dimensional (3D) WN nanosheets. Therefore, 2D and 3D films can simultaneously grow depending upon the concentration of the precursor. At low NH_3 concentrations (12 - 25%), the 3D growth is inhibited

and the products are 2D WN layers. When the NH_3 concentration increases to more than 25%, the 3D structure with flower-like vertical growth dominates (Figure 2c and Figure S5). The NH_3 concentration dependency of WN growth is summarized in Figure 2d. Our result suggests that a transition from 2D to 3D growth exists in the CVD WN growth, and 2D ultrathin WN could only be prepared at low NH_3 concentration.

The deposition of 2D WN crystal on substrates allows the investigation of its intrinsic mechanical properties. As-grown WN films on 285 nm SiO_2/Si substrates are coated with a thin layer of poly(methyl methacrylate) (PMMA) and subsequently the oxide layers are etched in a diluted buffered oxide etchant (BOE). The films are rinsed several times and transferred on Si substrates pre-patterned with 1 μm-diameter well arrays. The removal of PMMA layer in acetone solution are done with special care to ensure the suspended WN films on wells remain undamaged.

Young's moduli of the WN films are measured by AFM-based indentation experiments. Before the indentation, the surface morphologies and heights of WN films are measured in non-contact mode. The AFM tip is brought into contact with the center of the film suspending on the well and indented with a load causing a constant displacement rate. The load is then reversed and the whole process is repeated for several cycles. Figure 3b shows the measured force-deformation curves for repeated indentation with increasing force on the same position of a 12 nm thick WN sample. The almost completely overlapping curves indicate that there is no slippage or rupture and the membrane deformation is fully reversible during the measurements.

The displacement of the center of the film could be calculated by $\delta = \Delta Z_{piezo} - F/k$, where ΔZ_{piezo} is the displacement of the piezo and F/k is the deflection of the cantilever with k (2 N/m) representing the spring constant of the cantilever. Considering the three-fold rotation symmetry of hexagonal WN and the circular shape of the wells, the mechanical properties of the 2D WN sample

are therefore isotropic. It is noted that a pretension exists in the suspended film due to van der Waals interaction between WN and the substrate. For a small load, the force varies linearly with the displacement. When the load is large enough and the stress is significantly greater than the pretension of the film, the force and displacement are expected to follow a cubic relationship.[35] Thus the load can be approximately expressed as

$$F = (\sigma_0^{2D}\pi)\delta + \left(E^{2D}\frac{q^3}{r^2}\right)\delta^3 \quad (1)$$

where δ is the indentation depth at the center point, σ_0^{2D} is the pretension in the film, r is the radius of the suspended film, E^{2D} is the 2D elastic modulus and q is a dimensionless constant given as $q = 1/(1.05\text{-}0.15\nu\text{-}0.16\nu^2)$, with $\nu = 0.25$ is the Poisson ratio of bulk WN.[36]

Figure 4 shows representative experimental force-deformation curves for 4.5 nm and 12 nm thick suspended WN. A least-squares fit of equation 1 to the experimental data gives the pretension σ_0^{2D} and the 2D elastic modulus E^{2D}. The fitted curves (solid lines in Figure 4) agree well with the experimental data, indicating that equation 1 is a reliable model for estimating the relationship of force and displacement. The 2D elastic moduli of 4.5 nm and 12 nm thick WN are measured to be 1804 and 4490 N/m, respectively. To compare the modulus of WN with other different 2D layers and some conventional bulk materials, the 2D modulus has to be converted to the 3D modulus. The 3D Young's modulus E_{Young} is obtained by dividing the 2D elastic modulus by the film thickness. The corresponding values are 4.0×10^2 and 3.7×10^2 GPa for the 4.5 and 12 nm thick WN films, respectively. Further nanoidentation experiments suggests that there is no obvious difference of the E_{Young} for WN with thicknesses above 4.5 nm. In other words, the Young's modulus E_{Young} of WN is approximately independent of the film thickness. Figure S6 shows the typical force-deformation curve for the thinnest WN film (3 nm-thick) prepared by our CVD method. Fitting of equation 1 to the experimental data gives the Young's modulus to be 2.6×10^2

GPa. It is noted that the thinnest 3 nm WN film has a much smaller Young's modulus compared with thicker WN films. The surface of WN inevitably undergo slightly oxidation when exposed in air. XPS analysis of the WN films (Figure S7) demonstrates that the 3 nm thick WN contains significantly more oxidation induced defects as compared to thicker WN (with the same exposure time in air before XPS test). Surface oxygen defects will be a higher percentage of the volume of the material for the 3 nm thick films, which could result in the much smaller Young's modulus. Similar reductions of Young's moduli are also reported in defective ultrathin (1-5 layer) graphene and h-BN films.[37-38] Although there are some other reports that the reduction of interlayer sliding or stacking defects leads to the increment of Young's modulus in monolayer MoS_2 as compared with multilayers.[29, 39] However, this factor is not applicable in 2D WN which is not a van der Waals layered material.

Statistical analysis based on different samples gives the Young's modulus E_{Young} of few-layer WN (equal to or thicker than 4.5 nm) to be $3.9 \times 10^2 \pm 1.6 \times 10^2$ GPa, where the values before and after ± are the average value and the standard deviation (error) of E_{Young}, respectively. The average Young's modulus of our CVD grown few-layer WN is smaller than but close to the reported experimentally measured values of bulk hexagonal WN (ranging from 4.0×10^2 to 4.3×10^2 GPa).[36, 40] This may suggest that the surface effect does not significantly influence the Young's modulus of CVD grown few-layer WN. The theoretical Young's moduli for various species of tungsten nitride (W_xN_y) were investigated by density functional theory.[41-42] For stoichiometric tungsten nitride (W_xN_x), the authors reported Young's moduli of 4.2×10^2 to 4.5×10^2 GPa for hexagonal W_1N_1. Considering the surface dangling bonds and other surface effects,[43] the modulus of ultrathin WN should be smaller than the above reported theoretical values. Our experimental

average modulus value (3.9×10^2 GPa) for 4.5 - 12 nm WN is close to the theoretical values of stoichiometric hexagonal W_1N_1.

Figure 5 summarizes the reported experimental values of Young's moduli of different 2D materials. In comparison with other 2D members, few-layer 2D WN has a Young's modulus lower than that of graphene and h-BN,[44-45] but comparable with the best reported values of MoS_2, BP and Mxene $Ti_3C_2T_x$,[29, 46-47] and higher than that of most other 2D films including graphene oxide, WSe_2, GaS etc.[30, 48-49] The higher average E_{Young} of few-layer WN may indicate promise of having the material with the third highest modulus among the families of 2D materials. However, variation exists which is possibly due to CVD growth or sample transfer of the WN material. Further refinements to these processes would likely reduce the error.

3. Conclusion

In conclusion, we demonstrate the CVD growth of ultrathin 2D WN crystals on SiO_2/Si substrates. HRTEM, SAED and XPS confirm that the as-grown samples are highly crystalline hexagonal WN. The WN thickness could be tuned by the concentration of NH_3 during the CVD reaction. A 2D to 3D growth transition is observed with enhanced NH_3 concentration. The 2D WN films show a Young's modulus which is comparable with the best experimental reported values in 2D family except graphene and h-BN. The growth method presented here may also be applied for developing other 2D transition metal nitride crystals with versatile functionalities.

4. Experimental Section

Chemical vapor deposition of ultrathin WN crystals: The synthesis of ultrathin WN was conducted in a CVD system equipped with a 1-inch out-diameter fused quartz tube. WO_3 (0.7 g) and NaCl powders (0.2 g) were intimately mixed in an alumina crucible and then loaded in the center of the furnace. 285 nm SiO_2/Si chips was used as substrate and positioned slightly above the powder mixture with the polished side faced down. The furnace is heated to 800 °C in 16 min with 80 sccm (standard cubic centimeters per minute) Ar and 12 sccm H_2 as carrier gases. Then NH_3 with different concentrations was introduced into the system to allow the reaction. After 12 min growth, NH_3 was turned off and the sample was cooled rapidly under the protection of 200 sccm Ar and 12 sccm H_2. The as-grown WN sample on substrates were washed with flowing ethanol or water to remove possible absorbed salt on the SiO_2/Si chips.

Transfer of WN samples: For TEM and AFM measurement, the sample grown on 285 nm SiO_2/Si was coated by a thin poly (methyl methacrylate) (PMMA) layer, and then shifted to a diluted BOE solution to etch the 285 nm SiO_2 layer. The PMMA film-supported sample was rinsed several times in DI water and then picked up either by a TEM grid or a pre-patterned Si chip, for TEM or AFM indentation measurement, respectively. Finally, the PMMA layers were removed with acetone.

Sample characterizations: XPS spectra were collected on a PHI Quantera II spectrometer using monochromatic Al-Kα ($h\upsilon$ = 1486.6 eV) radiation. The energy calibrations were made against the C 1s peak to eliminate the charging of the sample during analysis. AFM images were taken using the Asylum Research Cypher AFM in tapping mode. HRTEM images and SAED patterns were taken by a JEOL JEM-2100 operated at 200 kV.

AFM-based nano-indentation experiment: The as prepared WN layers with different thicknesses were transferred and suspended over 1 micron circular wells etched into the SiO_2/Si substrates (285 nm thick SiO_2 on Si). The WN layers were mechanically characterized by nanoindentation in an Asylum Research MFP-3D AFM with a Si tip with a nominal radius of 9 nm and cantilever spring constant of about 2 N/m. The surface morphologies were measured in non-contacting mode while the indentations were performed in contacting mode by placing the AFM tip at the center of the well. Constant displacement rate was applied to test the mechanical testing which followed the load reversal.

Supporting Information

Supporting Information is available from the Wiley Online Library or from the author.

Acknowledgements

H.W and E.J.S contributed equally to this work. E.J.S and G.M acknowledge the help of Dr. Kenneth Strawhecker and Dr. John LaScala of ARL for their valuable input and guidance in performing the AFM indentation of the thin films, respectively. This work was performed under Cooperative Research and Development Agreement (ARL CRADA No. 15-57) and Joint Work Statement (ARL JWS No. 15-57-01) between the United States Army Research Laboratory, USA and Nanyang Technological University, Singapore entitled ‘Development of Novel and Emergent Nanomaterials beyond Graphene’.

Conflict of Interest

The authors declare no conflict of interest.

Received: ((will be filled in by the editorial staff))
Revised: ((will be filled in by the editorial staff))
Published online: ((will be filled in by the editorial staff))

References

[1] M. Chhowalla, H. S. Shin, G. Eda, L.-J. Li, K. P. Loh, H. Zhang, *Nature Chemistry* **2013**, 5, 263.
[2] B. Anasori, M. R. Lukatskaya, Y. Gogotsi, *Nature Reviews Materials* **2017**, 2, 16098.
[3] M. Naguib, V. N. Mochalin, M. W. Barsoum, Y. Gogotsi, *Adv Mater* **2014**, 26, 992.
[4] W. Choi, N. Choudhary, G. H. Han, J. Park, D. Akinwande, Y. H. Lee, *Mater Today* **2017**, 20, 116.
[5] G. R. Bhimanapati, Z. Lin, V. Meunier, Y. Jung, J. Cha, S. Das, D. Xiao, Y. Son, M. S. Strano, V. R. Cooper, *Acs Nano* **2015**, 9, 11509.
[6] C. Xu, L. Wang, Z. Liu, L. Chen, J. Guo, N. Kang, X.-L. Ma, H.-M. Cheng, W. Ren, *Nat Mater* **2015**, 14, 1135.
[7] Z. Y. Al Balushi, K. Wang, R. K. Ghosh, R. A. Vila, S. M. Eichfeld, J. D. Caldwell, X. Qin, Y. C. Lin, P. A. DeSario, G. Stone, S. Subramanian, D. F. Paul, R. M. Wallace, S. Datta, J. M. Redwing, J. A. Robinson, *Nat Mater* **2016**, 15, 1166.
[8] J. Wu, H. Yuan, M. Meng, C. Chen, Y. Sun, Z. Chen, W. Dang, C. Tan, Y. Liu, J. Yin, Y. Zhou, S. Huang, H. Q. Xu, Y. Cui, H. Y. Hwang, Z. Liu, Y. Chen, B. Yan, H. Peng, *Nat Nanotechnol* **2017**, 12, 530.
[9] J. Ji, X. Song, J. Liu, Z. Yan, C. Huo, S. Zhang, M. Su, L. Liao, W. Wang, Z. Ni, Y. Hao, H. Zeng, *Nature Communications* **2016**, 7, 13352.
[10] B. Zhao, W. Dang, Y. Liu, B. Li, J. Li, J. Luo, Z. Zhang, R. Wu, H. Ma, G. Sun, Y. Huang, X. Duan, X. Duan, *J Am Chem Soc* **2018**, 140, 14217.
[11] F. Wang, T. Gao, Q. Zhang, Z.-Y. Hu, B. Jin, L. Li, X. Zhou, H. Li, G. Van Tendeloo, T. Zhai, *Adv Mater* **2019**, 31, 1806306.
[12] R. Cheng, Y. Wen, L. Yin, F. Wang, F. Wang, K. Liu, T. A. Shifa, J. Li, C. Jiang, Z. Wang, J. He, *Adv Mater* **2017**, 29, 1703122.
[13] L. Liu, J. Wu, L. Wu, M. Ye, X. Liu, Q. Wang, S. Hou, P. Lu, L. Sun, J. Zheng, L. Xing, L. Gu, X. Jiang, L. Xie, L. Jiao, *Nat Mater* **2018**, 17, 1108.
[14] P. Urbankowski, B. Anasori, T. Makaryan, D. Er, S. Kota, P. L. Walsh, M. Zhao, V. B. Shenoy, M. W. Barsoum, Y. Gogotsi, *Nanoscale* **2016**, 8, 11385.
[15] X. Xiao, H. Yu, H. Jin, M. Wu, Y. Fang, J. Sun, Z. Hu, T. Li, J. Wu, L. Huang, Y. Gogotsi, J. Zhou, *Acs Nano* **2017**, 11, 2180.
[16] X. Xiao, P. Urbankowski, K. Hantanasirisakul, Y. Yang, S. Sasaki, L. Yang, C. Chen, H. Wang, L. Miao, S. H. Tolbert, S. J. L. Billinge, H. D. Abruña, S. J. May, Y. Gogotsi, *Adv Funct Mater* **2019**, 0, 1809001.
[17] F. Lévy, P. Hones, P. Schmid, R. Sanjinés, M. Diserens, C. Wiemer, *Surface and coatings technology* **1999**, 120, 284.
[18] D. Papaconstantopoulos, W. Pickett, B. Klein, L. Boyer, *Phys Rev B* **1985**, 31, 752.
[19] J. S. Becker, R. G. Gordon, *Appl Phys Lett* **2003**, 82, 2239.

[20] T. Polcar, N. M. G. Parreira, A. Cavaleiro, *Wear* **2007**, 262, 655.
[21] Z. Wang, V. Kochat, P. Pandey, S. Kashyap, S. Chattopadhyay, A. Samanta, S. Sarkar, P. Manimunda, X. Zhang, S. Asif, A. K. Singh, K. Chattopadhyay, C. S. Tiwary, P. M. Ajayan, *Adv Mater* **2017**, 29, 1700364.
[22] H. Wang, X. Huang, J. Lin, J. Cui, Y. Chen, C. Zhu, F. Liu, Q. Zeng, J. Zhou, P. Yu, X. Wang, H. He, S. H. Tsang, W. Gao, K. Suenaga, F. Ma, C. Yang, L. Lu, T. Yu, E. H. T. Teo, G. Liu, Z. Liu, *Nature Communications* **2017**, 8, 394.
[23] H. Wang, Y. Chen, M. Duchamp, Q. Zeng, X. Wang, S. H. Tsang, H. Li, L. Jing, T. Yu, E. H. T. Teo, Z. Liu, *Adv Mater* **2018**, 30, 1704382.
[24] J. Zhou, J. Lin, X. Huang, Y. Zhou, Y. Chen, J. Xia, H. Wang, Y. Xie, H. Yu, J. Lei, D. Wu, F. Liu, Q. Fu, Q. Zeng, C.-H. Hsu, C. Yang, L. Lu, T. Yu, Z. Shen, H. Lin, B. I. Yakobson, Q. Liu, K. Suenaga, G. Liu, Z. Liu, *Nature* **2018**, 556, 355.
[25] S. Li, S. Wang, D.-M. Tang, W. Zhao, H. Xu, L. Chu, Y. Bando, D. Golberg, G. Eda, *Applied Materials Today* **2015**, 1, 60.
[26] K. Chen, Z. Chen, X. Wan, Z. Zheng, F. Xie, W. Chen, X. Gui, H. Chen, W. Xie, J. Xu, *Adv Mater* **2017**, 29, 1700704.
[27] J. H. Sung, H. Heo, S. Si, Y. H. Kim, H. R. Noh, K. Song, J. Kim, C.-S. Lee, S.-Y. Seo, D.-H. Kim, H. K. Kim, H. W. Yeom, T.-H. Kim, S.-Y. Choi, J. S. Kim, M.-H. Jo, *Nat Nanotechnol* **2017**, 12, 1064.
[28] S. Bertolazzi, J. Brivio, A. Kis, *Acs Nano* **2011**, 5, 9703.
[29] A. Castellanos‐Gomez, M. Poot, G. A. Steele, H. S. van der Zant, N. Agraït, G. Rubio‐Bollinger, *Adv Mater* **2012**, 24, 772.
[30] J. W. Suk, R. D. Piner, J. An, R. S. Ruoff, *Acs Nano* **2010**, 4, 6557.
[31] M. Wen, Q. Meng, W. Yu, W. Zheng, S. Mao, M. Hua, *Surface and Coatings Technology* **2010**, 205, 1953.
[32] M. Nagai, K. Kishida, *Appl Surf Sci* **1993**, 70–71, Part 2, 759.
[33] D. K. Nandi, U. K. Sen, S. Sinha, A. Dhara, S. Mitra, S. K. Sarkar, *Physical Chemistry Chemical Physics* **2015**, 17, 17445.
[34] H. R. Rasouli, N. Mehmood, O. Cakiroglu, T. S. Kasirga, *Nanoscale* **2019**, 11, 7317.
[35] U. Komaragiri, M. R. Begley, J. G. Simmonds, *Journal of Applied Mechanics* **2005**, 72, 203.
[36] H. Peter, M. Nicolas, R. Manfred, L. Francis, *Journal of Physics D: Applied Physics* **2003**, 36, 1023.
[37] G. López-Polín, C. Gómez-Navarro, V. Parente, F. Guinea, Mikhail I. Katsnelson, F. Pérez-Murano, J. Gómez-Herrero, *Nature Physics* **2014**, 11, 26.
[38] L. Song, L. Ci, H. Lu, P. B. Sorokin, C. Jin, J. Ni, A. G. Kvashnin, D. G. Kvashnin, J. Lou, B. I. Yakobson, P. M. Ajayan, *Nano Lett* **2010**, 10, 3209.
[39] K. Liu, Q. Yan, M. Chen, W. Fan, Y. Sun, J. Suh, D. Fu, S. Lee, J. Zhou, S. Tongay, J. Ji, J. B. Neaton, J. Wu, *Nano Lett* **2014**, 14, 5097.
[40] C. Wang, Q. Tao, S. Dong, X. Wang, P. Zhu, *Inorganic chemistry* **2017**, 56, 3970.
[41] Z. Kang, H. Y. He, R. Ding, J. Chen, B. C. Pan, *Cryst. Growth Des.* **2018**, 18, 2270.
[42] D. V. Suetin, I. R. Shein, A. L. Ivanovskii, *physica status solidi (b)* **2008**, 245, 1590.
[43] A. I. Fedorchenko, A.-B. Wang, H. H. Cheng, *Appl Phys Lett* **2009**, 94, 152111.
[44] A. Falin, Q. Cai, E. J. G. Santos, D. Scullion, D. Qian, R. Zhang, Z. Yang, S. Huang, K. Watanabe, T. Taniguchi, M. R. Barnett, Y. Chen, R. S. Ruoff, L. H. Li, *Nature Communications* **2017**, 8, 15815.

[45] C. Lee, X. Wei, J. W. Kysar, J. Hone, *Science* **2008**, 321, 385.
[46] J.-Y. Wang, Y. Li, Z.-Y. Zhan, T. Li, L. Zhen, C.-Y. Xu, *Appl Phys Lett* **2016**, 108, 013104.
[47] A. Lipatov, H. Lu, M. Alhabeb, B. Anasori, A. Gruverman, Y. Gogotsi, A. Sinitskii, *Sci Adv* **2018**, 4, eaat0491.
[48] R. Zhang, V. Koutsos, R. Cheung, *Appl Phys Lett* **2016**, 108, 042104.
[49] B. Chitara, A. Ya'akobovitz, *Nanoscale* **2018**, 10, 13022.
[50] L. Guo, H. Yan, Q. Moore, M. Buettner, J. Song, L. Li, P. T. Araujo, H.-T. Wang, *Nanoscale* **2015**, 7, 11915.
[51] J. Tao, W. Shen, S. Wu, L. Liu, Z. Feng, C. Wang, C. Hu, P. Yao, H. Zhang, W. Pang, X. Duan, J. Liu, C. Zhou, D. Zhang, *Acs Nano* **2015**, 9, 11362.

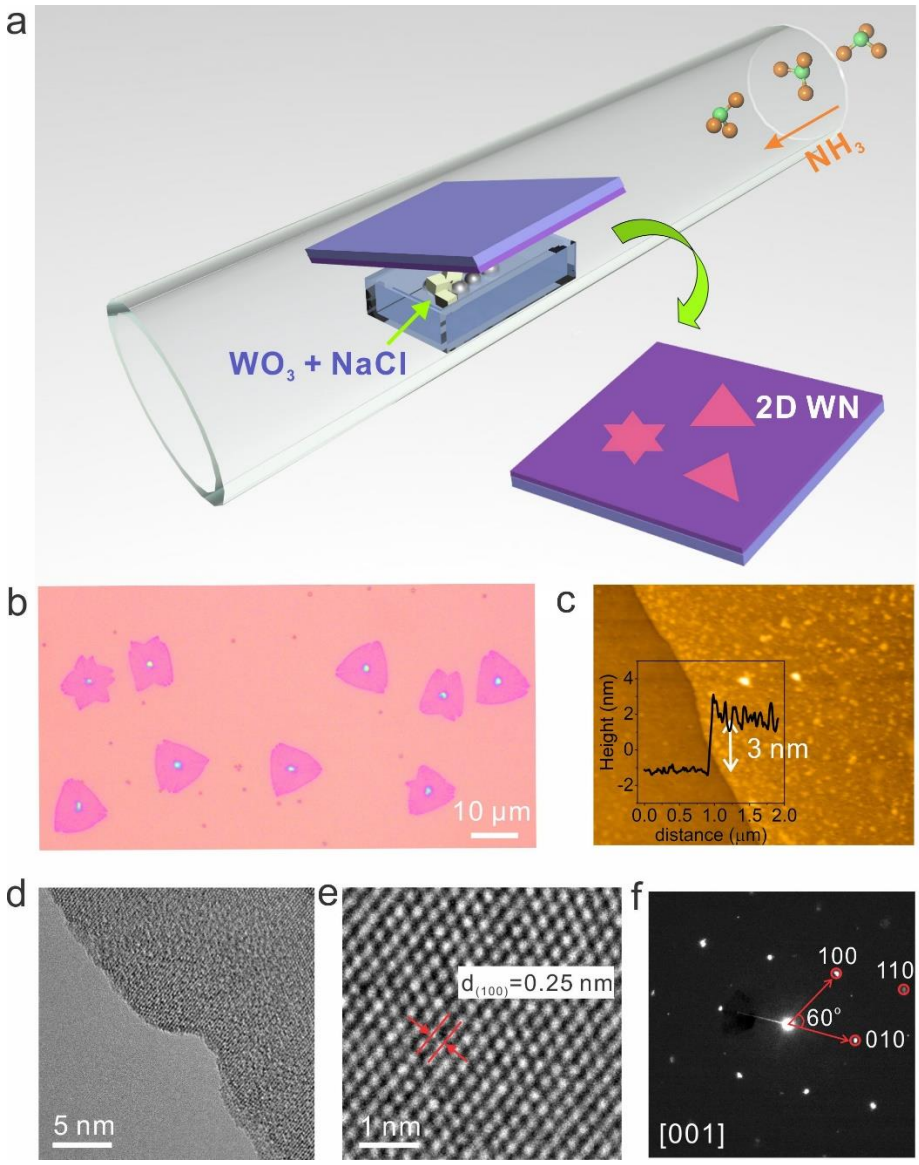

Figure 1. (a) Illustration of the CVD synthesis of ultrathin WN. (b) Optical image of ultrathin WN crystals deposited on a SiO_2/Si substrate. (c) AFM measurement indicates the typical thickness of WN is 3 nm (inset: AFM height profile). (d) A TEM image shows the edge of a transferred ultrathin WN layers. (e) A high-magnified TEM image shows the (100) lattice of WN. (f) SAED pattern of WN.

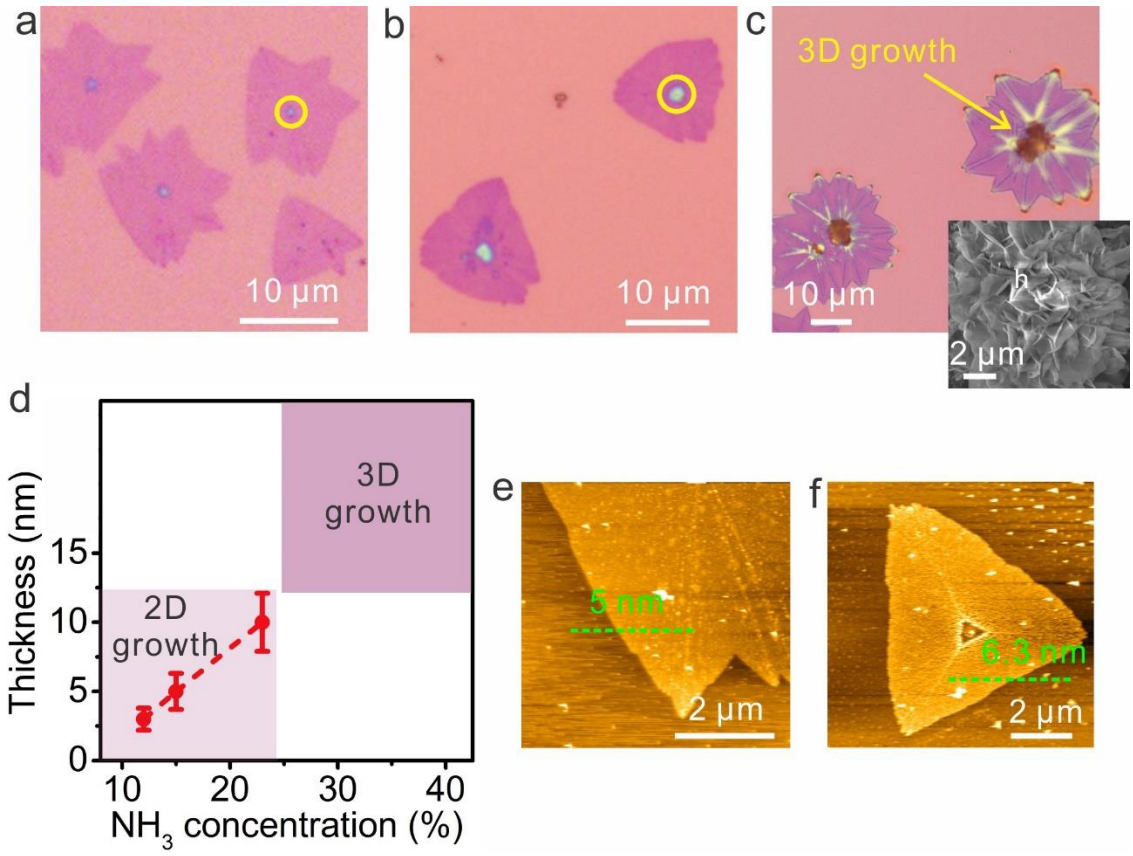

Figure 2. Transition from 2D to 3D growth in WN. (a-c) Optical images of the grown WN with increased ammonia concentration. The yellow circles in Figure 2a and 2b indicate the nucleation sites. The lower inset of Figure 2c shows a SEM image of the 3D nanosheets grown at the center of 2D WN. (d) Line plot of WN thickness versus ammonia concentration. A 2D to 3D growth transition occurs with increased ammonia concentration. (e, f) AFM images of WN crystals with 5 nm (e) and 6.3 nm (f) thicknesses.

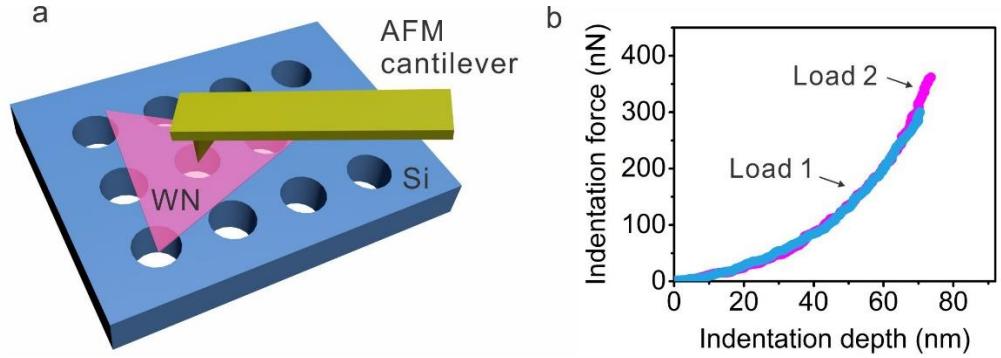

Figure 3. (a) Schematic illustration of the nanoindentation experiment setup. The AFM tip is firstly located at the center of a well covered by a WN film and then slowly lowered during the indentation. (b) Consecutive force-deformation curves of a 12 nm thick WN film under different loads.

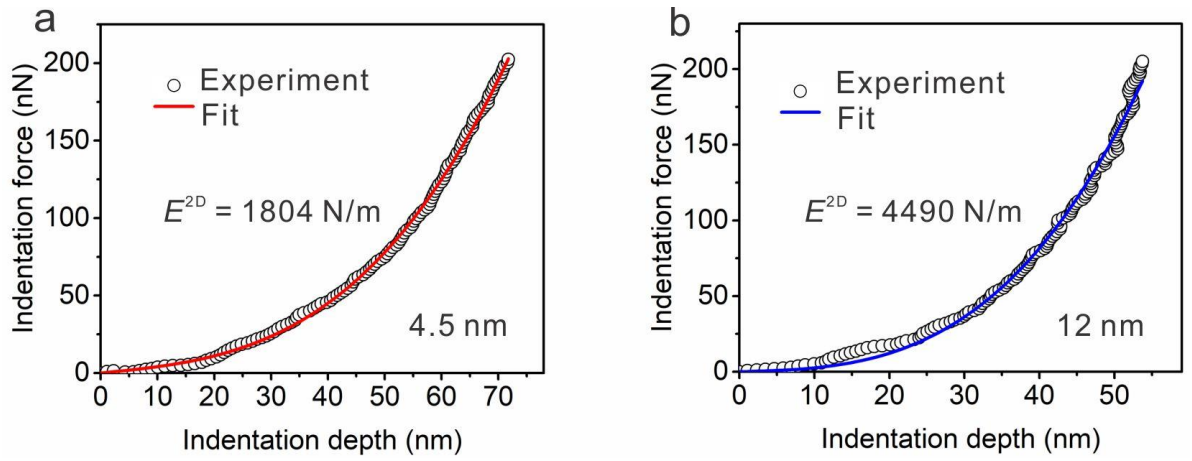

Figure 4. Typical experimental force-deformation data and the corresponding fitting curves for WN films with (a) 4.5 nm and (b) 12 nm in thickness. The 2D moduli are 1804 and 4490 N/m for 4.5 nm and 12 nm thick WN, corresponding to 3D Young's moduli of 4.0×10^2 and 3.7×10^2 Gpa, respectively.

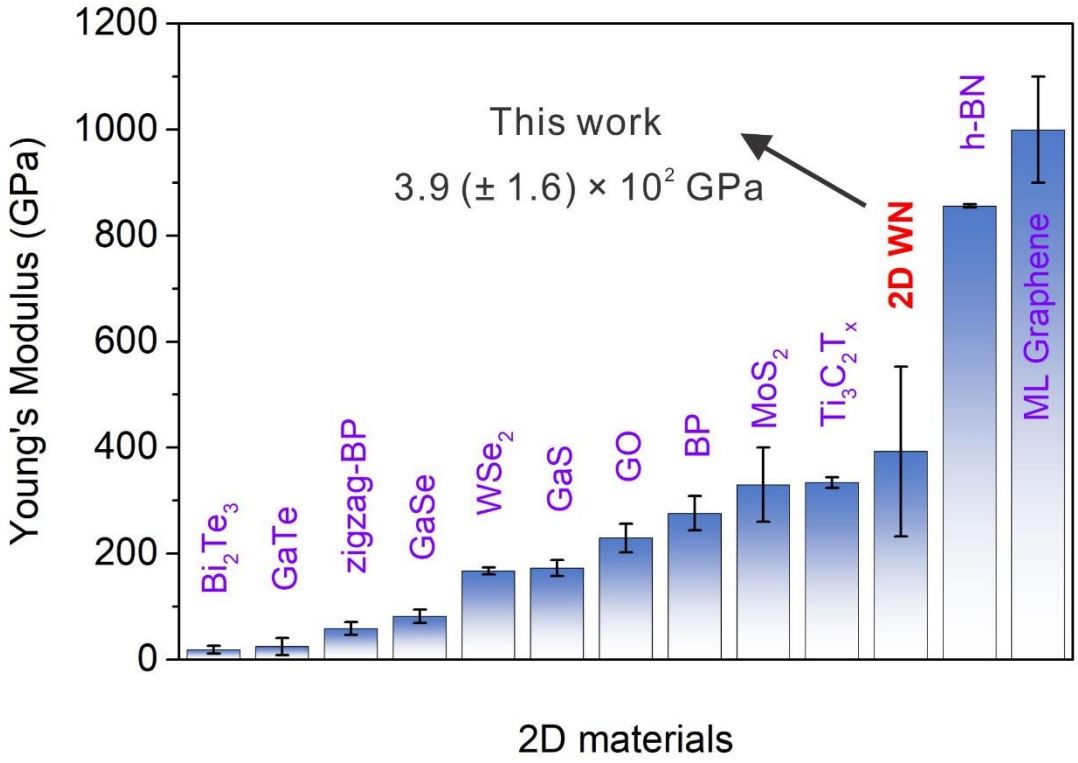

Figure 5. Comparison of the experimental 3D Young's moduli for several 2D few-layer materials: Bi_2Te_3,[50] GaTe,[49] zigzag-BP,[51] GaSe,[49] WSe_2,[48] GaS,[49] GO,[30] BP,[46] MoS_2,[29] $Ti_3C_2T_x$,[47] 2D WN and h-BN.[44] Monolayer graphene which exhibits the largest Young's modulus of 1.0 × 10^3 GPa[45] is also included as a reference.